Pseudomonas syringae type III effector HopAF1 suppresses plant immunity by targeting methionine recycling to block ethylene induction

Erica J. Washington[a], M. Shahid Mukhtar[a,1], Omri M. Finkel[a], Li Wan[a], Mark J. Banfield[b], Joseph J. Kieber[a], and Jeffery L. Dangl[a,c,d,e,f,2]

[a]Department of Biology, University of North Carolina, Chapel Hill, NC 27599; [b]Department of Biological Chemistry, John Innes Centre, Norwich NR4 7UH, United Kingdom; [c]Howard Hughes Medical Institute, University of North Carolina, Chapel Hill, NC 27599; [d]Curriculum in Genetics and Molecular Biology, University of North Carolina, Chapel Hill, NC 27599; [e]Department of Microbiology and Immunology, University of North Carolina, Chapel Hill, NC 27599; and [f]Carolina Center for Genome Sciences, University of North Carolina, Chapel Hill, NC 27599

Contributed by Jeffery L. Dangl, May 4, 2016 (sent for review February 21, 2016; reviewed by Sheng Yang He and Mary Beth Mudgett)

HopAF1 is a type III effector protein of unknown function encoded in the genomes of several strains of *Pseudomonas syringae* and other plant pathogens. Structural modeling predicted that HopAF1 is closely related to deamidase proteins. Deamidation is the irreversible substitution of an amide group with a carboxylate group. Several bacterial virulence factors are deamidases that manipulate the activity of specific host protein substrates. We identified *Arabidopsis* methylthioadenosine nucleosidase proteins MTN1 and MTN2 as putative targets of HopAF1 deamidation. MTNs are enzymes in the Yang cycle, which is essential for the high levels of ethylene biosynthesis in *Arabidopsis*. We hypothesized that HopAF1 inhibits the host defense response by manipulating MTN activity and consequently ethylene levels. We determined that bacterially delivered HopAF1 inhibits ethylene biosynthesis induced by pathogen-associated molecular patterns and that *Arabidopsis mtn1 mtn2* mutant plants phenocopy the effect of HopAF1. Furthermore, we identified two conserved asparagines in MTN1 and MTN2 from *Arabidopsis* that confer loss of function phenotypes when deamidated via site-specific mutation. These residues are potential targets of HopAF1 deamidation. HopAF1-mediated manipulation of Yang cycle MTN proteins is likely an evolutionarily conserved mechanism whereby HopAF1 orthologs from multiple plant pathogens contribute to disease in a large variety of plant hosts.

Pseudomonas syringae | type III effectors | ethylene | Yang cycle | plant immune system

The Gram-negative bacterium *Pseudomonas syringae* causes disease in agronomically important crops such as tomatoes, tobacco, and beans and in the model plant *Arabidopsis thaliana*. *P. syringae* uses the type III secretion system to inject type III effector (T3E) proteins into the host to cause disease in plants (1). *P. syringae* mutants lacking the type III secretion system lack the ability to cause disease in hosts, demonstrating that the type III secretion system is a primary virulence determinant (2).

The immune response that plants use to protect themselves against pathogens consists of multiple layers. The first line of defense, often called "PAMP-triggered immunity" (PTI), begins with transmembrane pattern recognition receptors (PRRs) perceiving conserved molecular patterns from pathogens called "pathogen-associated molecular patterns" (PAMPs). Because these microbial signatures are not limited to pathogenic microbes, they also are referred to as "microbial-associated molecular patterns" (MAMPs) (3, 4). Commonly studied bacterial PAMPs/MAMPs are lipopolysaccharide, peptidoglycan, elongation factor Tu (EF-Tu), and flagellin (4). A 22-aa peptide derived from a conserved region of the N terminus of bacterial flagellin (flg22), FLS2, is sufficient for recognition by host PRRs (5, 6). Recognition of flg22 leads to a downstream signaling cascade that includes many components, such as an increase in callose deposition, up-regulation of defense gene expression, and an increase in ethylene biosynthesis (7–9).

T3Es from plant bacterial pathogens promote virulence. T3Es commonly contain sequences addressing specific eukaryotic subcellular localizations (10, 11) and enzymatic activities (12–17) that disrupt and/or suppress PTI. Known targets of T3Es include plasma membrane-localized receptor complexes (13, 18–23), downstream MAPK cascades (24, 25), the stability of defense-related transcripts (26), phytoalexin biosynthesis (27), and vesicle trafficking (28).

To overcome effector-mediated suppression of PTI, plants evolved an intracellular surveillance system. Plants deploy highly polymorphic intracellular receptors often referred to as "NB-LRR" or "NLR" proteins, named for their domain architecture, to detect effectors from a wide variety of plant pathogens. Specific NLR proteins are activated either by direct recognition of a specific effector or by indirect recognition of the action of an effector on a specific host protein. Either recognition mode leads to effector-triggered immunity, considered to be an amplified form of PTI that often includes a localized programmed cell-death response called the "hypersensitivity response" (HR) (29, 30).

Plant hormones are also key modulators of the host immune response. Significant cross-talk between the three main defense hormones in plants, salicylic acid, jasmonic acid, and gaseous

Significance

***Pseudomonas syringae* is a Gram-negative bacterium that uses a type III secretion system to inject type III effector (T3E) proteins into the host to cause disease in plants. Multiple *P. syringae* T3Es promote virulence by targeting immune system signaling pathways using diverse biochemical mechanisms. We provide evidence for a molecular function of the *P. syringae* T3E HopAF1. We demonstrate that the C-terminal region of HopAF1 has structural homology to deamidases. We demonstrate that an enzyme important for production of the gaseous signaling hormone ethylene is a target for HopAF1 and show that HopAF1 targets methylthioadenosine nucleosidase proteins MTN1 and MTN2 to dampen ethylene production during bacterial infection.**

Author contributions: E.J.W., O.M.F., M.J.B., and J.L.D. designed research; E.J.W. and O.M.F. performed research; M.S.M., L.W., and J.J.K. contributed new reagents/analytic tools; E.J.W., O.M.F., M.J.B., and J.L.D. analyzed data; and E.J.W., O.M.F., and J.L.D. wrote the paper.

Reviewers: S.Y.H., Michigan State University; and M.B.M., Stanford University.

The authors declare no conflict of interest.

Freely available online through the PNAS open access option.

[1]Present address: Department of Biology, University of Alabama at Birmingham, Birmingham, AL 35294.

[2]To whom correspondence should be addressed. Email: dangl@email.unc.edu.

This article contains supporting information online at www.pnas.org/lookup/suppl/doi:10.1073/pnas.1606322113/-/DCSupplemental.

ethylene, allows the plant to regulate its response to various classes of pathogens and herbivores (31).

Insights into T3E function have benefited from a combination of structural modeling and protein–protein screens to identify possible host targets and effects on host physiology. We found that the previously unstudied *P. syringae* T3E HopAF1 impacts host ethylene biosynthesis. The precise role of ethylene signaling and biosynthesis in the PTI response is debated, but T3Es are known to modulate plant ethylene responses (32, 33).

HopAF1 was identified as a T3E in *P. syringae* pv. *tomato* DC3000 (*Pto* DC3000) and *P. syringae* pv. *phaseolicola* 1448A race 6 via its HrpL-dependent transcriptional induction, a loosely defined N-terminal translocation signal sequence, and its ability to be translocated into plant cells via a type III secretion system (34). HopAF1 is widely distributed, and its presence has been confirmed in 11 of 19 strains of pathogenic *P. syringae* (35). There also are HopAF1 orthologs in other plant pathogens, such as AvrXv3 from *Xanthomonas campestris* pv. *euvesicatoria* (36, 37), *Ralstonia solanacearum*, and *Pseudomonas savastoni* and Aave_1373 from *Acidovorax citrulli* (38). The presence of HopAF1 in multiple strains of *P. syringae* and other plant pathogens suggests it plays an important role in virulence.

Here, we demonstrate that the C-terminal region of HopAF1 is predicted to have structural homology to bacterial deamidases, members of the papain-like superfamily (39), and contains conserved putative catalytic residues within the predicted fold. HopAF1 inhibits PTI responses in a manner dependent on the putative catalytic residues. Further, we show that HopAF1 interacts with the *Arabidopsis* methylthioadenosine nucleosidases MTN1 and MTN2 at the plant plasma membrane. MTNs are proteins in the Yang cycle, which is required for recycling methionine to support de novo ethylene biosynthesis. We demonstrate that the Yang cycle is required for the high levels of ethylene biosynthesis during pathogen attack. HopAF1 inhibits the PAMP-induced increase in ethylene biosynthesis. The Yang cycle is required for PTI-induced ethylene biosynthesis, and mutants in Yang cycle enzymes phenocopy the effect of HopAF1 delivery from *P. syringae*. Finally, we identified deamidation-mimicking variants in MTN1 and MTN2 that result in the loss of MTN activity. We propose a model in which HopAF1 deamidation of *Arabidopsis* MTNs results in the inhibition of the Yang cycle, and therefore ethylene biosynthesis, during the PAMP-induced defense response.

Results

Evidence for Three Gene-Duplication Events in HopAF1 Evolutionary History. We searched the Integrated Microbial Genomes (IMG) database (40) for HopAF1 homologs and found them in 148 sequenced bacterial genomes: 106 *Pseudomonas*, 36 *Xanthomonas*, four *Ralstonia*, and two *Acidovorax* genomes. They are found in two copies in 11 *Xanthomonas* and 21 *Pseudomonas* genomes.

Phylogenetic analysis (Fig. S1 *A* and *B*) clustered these homologs into three main groups, likely the consequence of two early duplication events. The first group includes the canonical HopAF1 gene and is present in *Xanthomonas*, *Pseudomonas*, and *Ralstonia*; the second group, which includes AvrXv3, is present in *Xanthomonas*, *Pseudomonas*, and *Acidovorax*; and the third group is exclusive to *Xanthomonas*. The three groups are found in all possible combinations of single and double copies in *Xanthomonas* genomes (Fig. S1*C*), with no apparent phylogenetic signal. The topology of the tree can be explained by two competing parsimonious models: that HopAF1 evolved and duplicated in *Xanthomonas*, wherein the majority of its diversity is represented, and was transferred horizontally to *Pseudomonas*, *Ralstonia*, and *Acidovorax* (model A), or that HopAF1 evolved and duplicated in a β-γ proteobacterial common ancestor and since then has been subject to reductive evolution eliminating most copies of the gene (model B).

A third, more recent duplication event likely took place within the canonical HopAF1 group in Pseudomonads. Both copies were retained in 13 of the genomes; the rest retained either one or the other copy (Fig. S1*C*). Interestingly, two *P. syringae* pathovars (pv. *pisi* and pv. *mori*) contain an AvrXv3 type gene in addition to a HopAF1 copy. The presence of this AvrXv3 type gene in these *Pseudomonas* pathovars can be seen either as evidence supporting the reductive evolution model (model B above) or as evidence for a separate horizontal gene-transfer event resulting in the transfer of the gene from *Xanthomonas* to Pseudomonads.

HopAF1 Contains a Putative C-Terminal Catalytic Domain. We used the BioInfoBank meta server and HHPred structural prediction programs to generate a model of the structure of HopAF1 from *Pto* DC3000 (41, 42). Homology searches predicted with high confidence that the C-terminal region (residues 130–284) of HopAF1 from *Pto* DC3000 is structurally related to CheD, a single-domain chemotaxis protein from *Thermotoga maritima* (Fig. 1*A*) (43).

We also generated a structural model for the divergent HopAF1 family member, AvrXv3 from *X. campestris* pv. *euvesicatoria*, which triggers the HR in tomatoes and peppers (36). Although HopAF1 and AvrXv3 are only 27% identical at the primary amino acid sequence level, modeling predicts that AvrXv3 also has structural homology to CheD (Fig. S2*A*). All known HopAF1 family members, except for the C-terminally truncated *P. syringae* pv. *actinidae* allele, contain predicted secondary structure elements homologous to CheD in these models (Fig. S2*B*).

CheD is a deamidase protein that activates methyl-accepting chemotaxis proteins (43). CheD is structurally related to the cytotoxic necrotizing factor family of bacterial deamidases (44, 45). Deamidation is a posttranslational modification used by multiple bacterial virulence factors to modify the function of eukaryotic host target proteins (39). Deamidation results in irreversible conversion of asparagine and glutamine residues to aspartic acid and glutamic acid, respectively. Bacterial deamidases require conserved histidine and cysteine residues for catalytic activity. Our modeling suggested that the C-terminal regions of both HopAF1 and AvrXv3 likely adopt a fold in which the positions of invariant catalytic residues for deamidation, cysteine and histidine, are conserved (Fig. 1*A* and Fig. S2*A*). These two residues are maintained in all known HopAF1 orthologs (Fig. S2*C*). Therefore, we predicted that these residues are critical for HopAF1 enzymatic function.

A third catalytic residue in deamidases coordinates the imidazole ring of histidine to ensure optimal orientation of the thiolate–imidazolium pair (39). We hypothesized that HopAF1 D154 may be involved in catalytic activity (Fig. 1 and Fig. S2*C*). Because of the limitations of structural modeling, the exact position of HopAF1 D154 cannot be confidently predicted. Therefore, we focused on the putative HopAF1 catalytic residues, C159 and H186.

HopAF1 Inhibits flg22-Induced Pathogen Growth Restriction, and This Inhibition Requires Its Putative Catalytic Residues. To determine if HopAF1 plays a role in virulence, we obtained a *Pto* DC3000 strain in which the *hopAF1* gene has been disrupted (46). We did not observe a significant growth defect in *Pto* DC3000Δ*hopAF1* (Fig. S3*A*). The lack of effect for a single T3E knockout is a common result for this strain and suggests functional redundancy. We next tested whether HopAF1 could enhance the growth of a weak pathogen. To do so, we generated estradiol-inducible HopAF1 transgenic *Arabidopsis* ecotype Col-0 plants expressing either wild-type HopAF1 or a double mutant in both the C159 and H186 putative catalytic residues ($HopAF1_{C159AH186A}$). Conditional expression of wild-type HopAF1 and $HopAF1_{C159AH186A}$ was evident 6 h after estradiol induction and was maintained for 48 h (Fig. S3*B*).

The removal of 28 T3Es by sequential mutagenesis from *Pto* DC3000 transformed this virulent strain into a weakly pathogenic derivative called "*Pto* DC3000D28E" that stimulates PTI

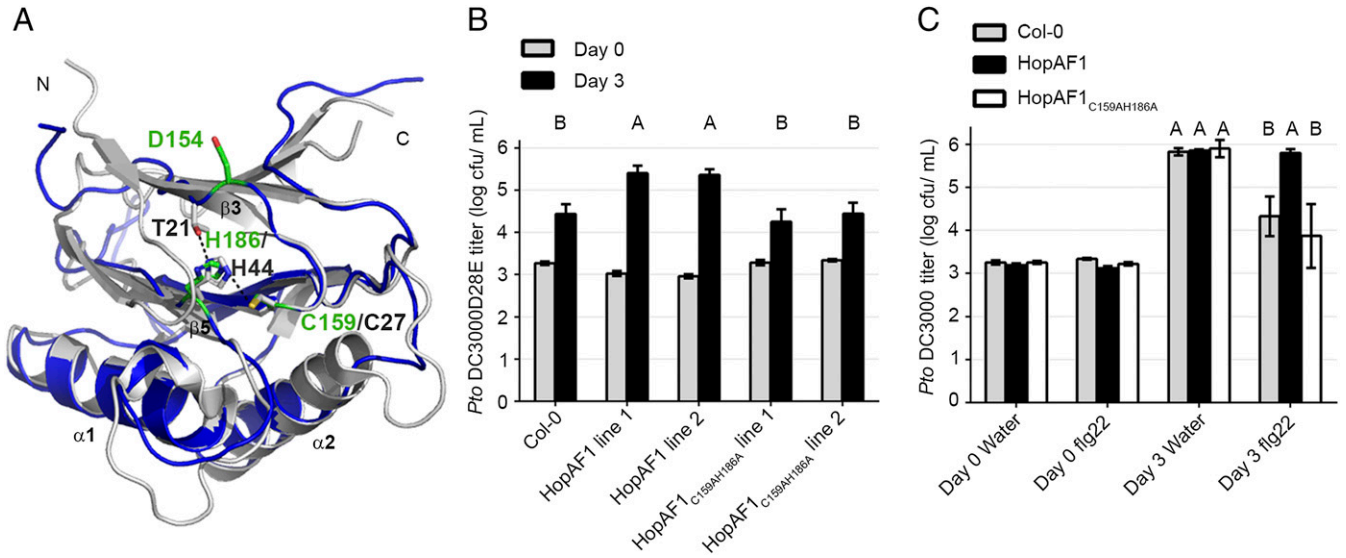

Fig. 1. HopAF1 putative catalytic residues in HopAF1 transgenic lines are required for an increase in susceptibility to a disarmed pathogen and inhibition of flg22-induced defense. (*A*) Homology model of the HopAF1 reference allele (blue) from *Pto* DC3000 residues 130–284 aligned with CheD (PDB ID code 2F9Z) (silver). The side chains of the putative catalytic residues of HopAF1 D154, C159, and H186 are shown in green. The side chains of the CheD catalytic residues C27, H44, and T21 are shown in silver. The N and C termini of the proteins are labeled, as are the key structural elements (α helix 1, α helix 2, β sheet 3, and β sheet 5). PyMOL was used to generate the figure. (*B*) Bacterial growth of *Pto* DC3000D28E in Col-0 plants and two independent transgenic lines expressing either estradiol-inducible HopAF1-cerulean-HA or estradiol-inducible $HopAF1_{C159AH186A}$-cerulean-HA was measured 0 and 3 d after hand-inoculation with bacteria (1×10^5 cfu/mL). Transgene expression was induced with 20 μM estradiol 24 h before bacterial inoculation. Error bars represent SEM. An ANOVA was performed among the day 3 samples, followed by Tukey's post hoc analysis ($P < 0.05$). The different letters indicate groups that differ significantly. (*C*) Col-0, estradiol-inducible HopAF1-cerulean-HA, and estradiol-inducible $HopAF1_{C159AH186A}$-cerulean-HA plants were sprayed with 20 μM estradiol for 12 h and then were infiltrated with 1 μM flg22 or water for 24 h before infiltration with 1×10^5 cfu/mL *Pto* DC3000. Bacterial growth was determined 0 and 3 d after bacterial inoculation. Error bars represent SEM. An ANOVA was performed among the day 3 samples, followed by Tukey's post hoc analysis ($P < 0.05$). The different letters indicate groups that differ significantly.

effectively (47). To determine if HopAF1 inhibits PTI, we measured the growth of *Pto* DC3000D28E in the HopAF1 and $HopAF1_{C159AH186A}$ transgenic lines 24 h after the induction of HopAF1 expression by estradiol treatment. We observed enhanced growth of *Pto* DC3000D28E in HopAF1-expressing transgenic lines compared with Col-0 plants, demonstrating that conditional HopAF1 expression allowed the enhanced growth of a weak pathogen when overexpressed *in planta* (Fig. 1*B* and Fig. S3*C*). The increase in bacterial growth in HopAF1 transgenic lines correlated with an increase in disease symptoms (Fig. S3*D*). The growth of *Pto* DC3000D28E in transgenic lines expressing the putative catalytic dead HopAF1 was similar to that in Col-0 plants (Fig. 1*B*), indicating that the increased host susceptibility in the HopAF1 transgenic lines requires the putative catalytic residues of HopAF1.

Pretreatment of *Arabidopsis* plants with flg22 diminishes susceptibility to subsequent infection with virulent pathogens such as *Pto* DC3000 (48). We examined flg22-induced disease resistance in Col-0 plants and in the HopAF1 transgenic lines to determine whether HopAF1 expression inhibits PTI. As expected, we observed reduced growth of *Pto* DC3000 on Col-0 plants treated with flg22 compared with water-treated plants at 3 d after treatment (Fig. 1*C*). This effect was suppressed in transgenic Col-0 plants expressing HopAF1 but not in transgenic Col-0 plants expressing $HopAF1_{C159AH186A}$ (Fig. 1*C* and Fig. S3*E*). We conclude that the expression of HopAF1 *in planta* suppresses PTI signaling induced by either *Pto* DC3000D28E or flg22 in a manner dependent on its putative catalytic residues.

HR Triggered by AvrXv3 in Tomato Is also Dependent on its Putative Catalytic Residues. AvrXv3 is recognized by, and elicits an HR in, tomato cultivar Florida 216 (Fla 216) but not tomato cultivar Florida 7060 (Fla 7060) (36). To determine if the putative catalytic residues of AvrXv3 are required for host recognition and the HR, we generated clones that allowed the constitutive overexpression of wild-type AvrXv3 and the AvrXv3 putative catalytic residue mutant, $AvrXv3_{H126A}$, with a C-terminal myc tag. We transiently expressed wild-type and mutant AvrXv3 in both tomato cultivars via *Agrobacterium*-mediated transfer DNA (T-DNA), measured their expression by immunoblot, and scored for the HR. Wild-type AvrXv3, but not $AvrXv3_{H126A}$, triggered the HR on Fla 216 (Fig. S4*A*). All proteins were expressed (Fig. S4*B*). These data suggest that the recognition of AvrXv3 in tomato requires H126 and further support the importance of the predicted catalytic activity in the HopAF1 T3E family.

HopAF1 Is Targeted to the Plasma Membrane via Acylation. The N termini of multiple HopAF1 orthologs contain putative sites for myristoylation (G2) and palmitoylation (C4) (Fig. S2*C*). Myristoylation is a eukaryotic-specific posttranslational modification that often is used in combination with palmitoylation to target proteins to the plasma membrane (49). Multiple *P. syringae* T3Es acylated and localized to the plasma membrane once delivered into plant cell by the type III secretion system (50–54).

We predicted that HopAF1 G2 and C4 motifs are required to target HopAF1 to the plasma membrane. To investigate this prediction, we generated a HopAF1 variant with mutations in the key residues, $HopAF1_{G2AC4S}$. We predicted that AvrXv3, which lacks the putative acylation sequence, would localize to the cytoplasm (Fig. S2*C*). We used confocal microscopy to detect transiently expressed estradiol-inducible HopAF1 and AvrXv3 in *Nicotiana benthamiana*. Both proteins were tagged on the C terminus with a cerulean-HA tag. We generated a plasma membrane marker, PLC2-YFP, as a localization control (55). Wild-type HopAF1-cerulean-HA colocalized at the plasma membrane with PLC2-YFP (Fig. 2*A*). In contrast, the acylation minus variant,

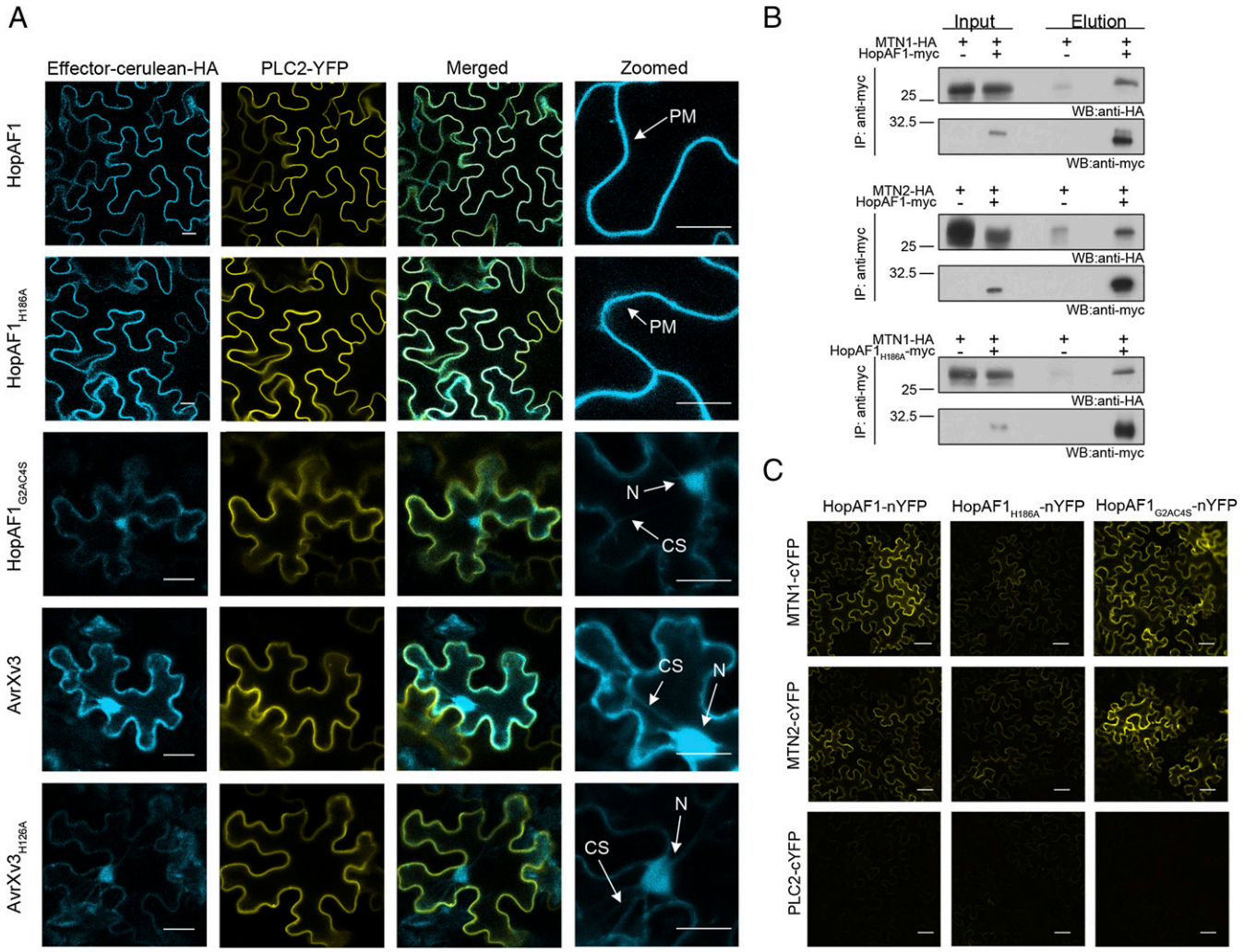

Fig. 2. HopAF1 interacts with Yang cycle proteins MTN1 and MTN2 at the plasma membrane. (*A*) Estradiol-inducible HopAF1-cerulean-HA, HopAF1$_{G2AC4S}$-cerulean-HA, HopAF1$_{H186A}$-cerulean-HA, AvrXv3-cerulean-HA, and AvrXv3$_{H126A}$-cerulean HA were expressed transiently in *N. benthamiana* using *Agrobacterium*-mediated transient transformations. Transgene expression was induced with 5 μM estradiol 3 d after bacterial infiltration. The localization of transiently expressed proteins was determined with scanning confocal laser microscopy 3 h after estradiol induction in *N. benthamiana* epidermal cells. PLC2-YFP is a marker for the plasma membrane localization. White arrows indicate the plasma membrane (PM), cytoplasmic streaming (CS), and nuclei (N). The zoomed images display only the cerulean channel. (Scale bars, 20 μm.) (*B*) Protein extracts from *N. benthamiana* leaves transiently expressing HopAF1-4x-myc, HopAF1$_{H186A}$-4x-myc, MTN1-HA, and MTN2-HA were collected 3 d after infiltration and were subjected to immunoprecipitation using anti-myc–coupled magnetic beads; 400 μg of input and a 50× concentrated elution fraction were analyzed by anti-HA and anti-myc immunoblots. (*C*) HopAF1-nYFP, HopAF1$_{H186A}$-nYFP, and HopAF1$_{G2AC4S}$-nYFP were transiently coexpressed with MTN1-cYFP, MTN2-cYFP, and PLC2-cYFP in *N. benthamiana* leaves using *Agrobacterium*-mediated transient transformation. Confocal microscopy was used to image the reconstituted YFP signal 3 d after infiltration. (Scale bars, 50 μm.)

HopAF1$_{G2AC4S}$-cerulean-HA, was localized to the plant cell cytoplasm (Fig. 2*A*). This cytoplasmic localization pattern overlapped with free YFP, a marker for nucleocytoplasmic-localized proteins (Fig. S5*A*). Wild-type AvrXv3 also was observed in the cytoplasm (Fig. 2*A*). Both HopAF1$_{H186A}$ and AvrXv3$_{H126A}$ localized as their respective wild-type proteins, suggesting that the putative catalytic activity of these HopAF1 orthologs is not required for their subcellular localization (Fig. 2*A*).

To confirm the confocal data, we performed cell fractionation assays with *N. benthamiana* tissues transiently expressing the constructs described above. We used ascorbate peroxidase (APX) and H$^+$-ATPase as markers for the soluble and membrane fractions, respectively, and as confirmation that the separation of the fractions was complete. We detected wild-type HopAF1 in the microsomal fraction, which contains the plasma membrane, but the acylation minus variant HopAF1$_{G2AC4S}$-cerulean-HA was found solely in the soluble fraction (Fig. S5*B*). AvrXv3 also was present in the soluble fraction. Catalytically inactive HopAF1$_{H186A}$ and AvrXv3$_{H126A}$ remained localized to the plasma membrane and soluble fraction, respectively (Fig. S5*B*). To diminish the chance of aberrant protein localization, we determined the lowest amount of *Agrobacterium* and estradiol necessary to detect HopAF1 via immunoblot (Fig. S5*C*). We also confirmed that we were assaying the localization of full-length HopAF1-cerulean-HA and that no band migrating at the expected apparent molecular weight of free soluble cerulean was present (Fig. S5*D*). We conclude that HopAF1 is targeted to the plant plasma membrane via the acylation signal sequence and that mutation of the putative catalytic residues does not affect this localization, even though HopAF1$_{H186A}$ has a virulence defect.

HopAF1 Associates with *Arabidopsis* MTN Proteins at the Plasma Membrane. We previously identified and confirmed *Arabidopsis* methylthioadenosine nucleosidase (MTN1; At4g38800) as a protein

that interacts with HopAF1 in a yeast two-hybrid screen (56). MTNs function in the methionine recycling pathway, also known as the "Yang cycle" (57). In *Arabidopsis*, two proteins, MTN1 and MTN2 (67% identical), are responsible for MTN activity (58). The Yang cycle regenerates methionine required to maintain high levels of ethylene biosynthesis when steady-state levels of methionine are limiting (Fig. S6*A*) (59). Therefore, we hypothesized that the Yang cycle, and MTN1 and MTN2, would be required for the PTI-triggered induction of ethylene biosynthesis and that disrupting the function of the *Arabidopsis* MTNs would dampen ethylene biosynthesis induced during PTI. Additionally, we predicted that the function of HopAF1 in virulence is to inhibit MTN function and block ethylene-dependent PTI.

To confirm the interaction of HopAF1 with MTN1 and MTN2, we performed coimmunoprecipitation studies in *N. benthamiana* leaves. We transiently coexpressed C-terminally myc-tagged HopAF1-myc with MTN1-HA or MTN2-HA. The cell lysates were incubated with anti-myc–conjugated beads. Bound MTN proteins then were detected with anti-HA immunoblots. We found that both MTN1-HA and MTN2-HA interacted with HopAF1-myc and that this binding did not require the HopAF1 putative catalytic residue, H186 (Fig. 2*B*). We conclude that HopAF1 interacts with *Arabidopsis* proteins MTN1 and MTN2 when transiently overexpressed in *N. benthamiana*.

Next we sought to determine where MTN1 and MTN2 localize within the plant cell. Cell fractionation and microscopy studies demonstrated that, when overexpressed, MTN1 and MTN2 can be found in the cytoplasm and at the plasma membrane of *N. benthamiana* epidermal cells (Fig. S6 *B* and *C*) (60). We investigated these potentially different localizations of HopAF1 and *Arabidopsis* MTNs using bimolecular fluorescence complementation (BiFC) experiments (61). We generated constructs with MTN1 and MTN2 fused at their C termini to the C-terminal half of YFP (MTN1-cYFP and MTN2-cYFP). HopAF1 variants were fused at the C terminus to the N-terminal half of YFP (HopAF1-nYFP). As a negative control, we assayed whether HopAF1-nYFP associated with PLC2-cYFP, a plasma membrane marker (55). Reconstitution of YFP, resulting in a fluorescent signal emitting light at 514 nm, occurred at the plasma membrane when wild-type HopAF1-nYFP was coexpressed in *N. benthamiana* cells with either MTN1-cYFP or MTN2-cYFP (Fig. 2*C*). However, there was no reconstitution of YFP when HopAF1-nYFP was coexpressed with PLC2-cYFP (Fig. 2*C*). Reconstitution at the plasma membrane was not dependent on the putative catalytic activity of HopAF1 (Fig. 2*C*). As is consistent with the presence of *Arabidopsis* MTNs in the cytoplasmic fraction (Fig. S6 *A* and *B*), the acylation minus HopAF1$_{G2AC4S}$-nYFP variant coexpressed with MTN1-cYFP or MTN2-cYFP reconstituted the YFP signal but did so in the cytoplasm (Fig. 2*C*). We conclude that wild-type HopAF1 and *Arabidopsis* MTNs interact specifically at the plasma membrane, as is consistent with the demonstrated localization of HopAF1 and with the observation that MTN1 and MTN2 may transiently localize to the plasma membrane via protein–protein interactions (60, 62).

HopAF1 Inhibits PAMP-Induced Ethylene Production. Recognition of flg22 triggers the activation of a MAPK cascade that leads to an increase in ethylene biosynthesis (7–9). The type III secretion system-deficient mutant *Pto* DC3000 *hrcC* triggers more ethylene biosynthesis than wild-type *Pto* DC3000 (Fig. S7*A*), suggesting that one or more components of the T3E suite from *Pto* DC3000 can suppress ethylene accumulation.

We established a system in which we could both induce ethylene biosynthesis with PAMPs and determine the effect of HopAF1 on this induction. To induce PAMP-mediated ethylene production, we used a *Pseudomonas fluorescens* strain (*Pfo*-1) lacking known T3Es but engineered to carry a functional type III secretion system as a delivery vehicle for PAMPs and, if desired, specific T3Es (63). *Pfo*-1 triggered an increase in ethylene production in *Arabidopsis* leaves (Fig. S7*B*). We transformed HopAF1 variants expressed from their native promoter into *Pfo*-1. All HopAF1 alleles were expressed equally (Fig. S7*C*) and were translocated as HopAF1-Δ79′AvrRpt2 fusion proteins into *Arabidopsis* RPS2 leaves (Fig. S7*D*) (64).

Leaves infected with *Pfo*-1 expressing HopAF1 inhibited the PAMP-induced ethylene biosynthesis compared with leaves infected with *Pfo*-1 or *Pfo*-1 carrying an empty vector control (Fig. 3*A*). Inhibition of ethylene production required the HopAF1 putative catalytic residue H186 (Fig. 3*B*). Notably, the inhibition of PAMP-induced ethylene production was not dependent on HopAF1 localization in the plasma membrane (Fig. 3*B*).

The Yang Cycle Is Required for PAMP-Induced Increase in Ethylene Biosynthesis. We predicted that HopAF1 suppression of PAMP-induced ethylene production would be phenocopied in mutants of Yang cycle intermediates. As noted above, there are two MTN paralogs in *Arabidopsis*, and it is likely that they function redundantly in the Yang cycle (65). MTN activity is required for maximal ethylene biosynthesis in tomatoes (66). The enzyme downstream of MTN in the Yang cycle, MTK, is also required for maximal levels of ethylene biosynthesis (59). We obtained *Arabidopsis mtn1* and *mtn2* mutants and generated the *mtn1 mtn2* double mutant (65). We demonstrated that high levels of ethylene were induced by *Pfo*-1 in either the *mtn1* or *mtn2* single mutants, consistent with these proteins functioning redundantly for Yang cycle-mediated PAMP-induced ethylene biosynthesis (Fig. 3*C*). However, in both the *mtk* single mutant and the *mtn1 mtn2* double mutant, *Pfo*-1 was unable to induce high levels of ethylene production, demonstrating that the Yang cycle is necessary for PAMP-induced ethylene production in this assay (Fig. 3*D*). These results are consistent with our hypothesis that HopAF1 can inhibit PAMP-induced ethylene biosynthesis by modulating or inhibiting the functions of *Arabidopsis* MTN1 and MTN2.

HopAF1 Inhibits MTN1 Activity in Vitro in a Manner Dependent on Its Putative Catalytic Residues. We used recombinant proteins purified from *Escherichia coli* to determine if HopAF1 can inhibit MTN1 function directly. We used circular dichroism to confirm that MTN1, 6xHis-HopAF1, and 6xHis-HopAF1$_{H186A}$ are folded (Fig. S8 *A* and *B*). We demonstrated that HopAF1 inhibited the ability of MTN1 to cleave its substrate (Fig. S8*C*) but HopAF1$_{H186A}$ did not (Fig. S8*D*). Furthermore, the proposed catalytic domain of HopAF1 (residues 130–284) was sufficient to inhibit MTN1 function (Fig. S8*D*). The Δ147HopAF1 truncated protein was not able to inhibit MTN1 function, suggesting that an essential part of the HopAF1 structure exists between residues 130 and 147 (Fig. S8*D*). These in vitro data suggest that HopAF1 inhibits PAMP-induced ethylene biosynthesis by directly inhibiting MTN1 activity.

Yang Cycle Mutants Are Impaired in Ethylene-Dependent Defense Responses. To determine the role of the Yang cycle in PTI, we assayed the susceptibility of *mtn1 mtn2* and *mtk* to *Pto* DC3000D28E (47). As a control, we used an ethylene-insensitive protein 2 (*ein2*)-null mutant (67). Ethylene-insensitive mutants allow enhanced growth of weak pathogens and are defective in flg22-mediated priming of the immune system (68, 69). *In planta* bacterial growth analyses show that Yang cycle mutants are more susceptible to *Pto* DC3000D28E, similar to *ein2* (Fig. 4). Additionally, the enhanced growth of *Pto* DC3000D28E in *mtn1 mtn2* plants was similar to levels of the same strain observed in transgenic plants expressing wild-type HopAF1 (Fig. 4).

Mutation of Two Conserved MTN Asparagine Residues to Deamidation Mimics Results in Loss of Function. We addressed whether the function of *Arabidopsis* MTNs could be perturbed by generating deamidation-mimicking mutations of conserved asparagine

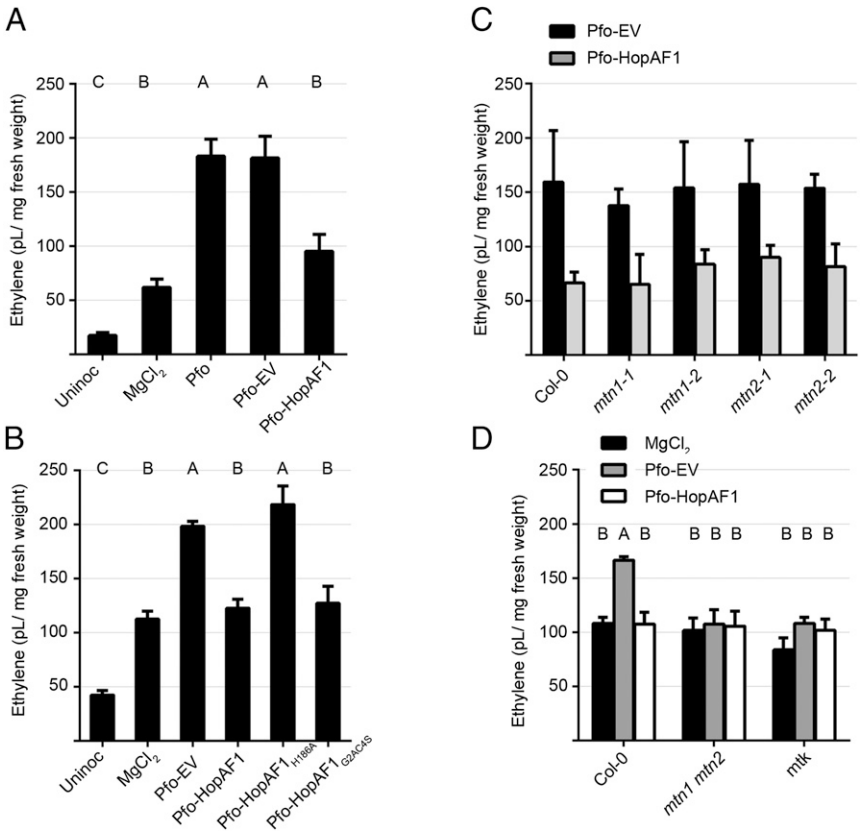

Fig. 3. HopAF1 inhibits ethylene biosynthesis and phenocopies *mtn1 mtn2* for a PTI-induced increase in ethylene biosynthesis. (*A*) *Arabidopsis* leaves were hand-infiltrated with $MgCl_2$ (vehicle control), *Pfo-1*, *Pfo-1* carrying the empty vector (EV), or *Pfo-1* expressing HopAF1. (*B*) In addition to the aforementioned treatments, *Arabidopsis* leaves were hand-infiltrated with *Pfo-1* expressing $HopAF1_{H186A}$ and *Pfo*-1 expressing $HopAF1_{G2AC4S}$. (*C*) Leaves of Col-0 plants and *Arabidopsis* mutants *mtn1-1*, *mtn1-2*, *mtn2-1*, and *mtn2-2* were hand-infiltrated with *Pfo-1* carrying the empty vector (EV) or with *Pfo-1* expressing wild-type, native promoter HopAF1. (*D*) Leaves of Col-0 and *Arabidopsis* mutants *mtn1-2 mtn2-2* and *mtk* were hand-infiltrated with $MgCl_2$, *Pfo-1* carrying the empty vector (EV), or *Pfo-1* expressing the wild-type native promoter HopAF1. In all experiments, the fresh weight of four leaves was measured 3 h post infiltration, and these leaves were sealed in a vial for 24 h before ethylene accumulation was measured. Letters represent treatments with significant difference according to the post hoc ANOVA Tukey's test ($P < 0.05$).

or glutamine residues. We found only three residues fully conserved across the evolutionary distance between plants and *E. coli* (70) that could be deamidase targets: $MTN1_{N113}$, $MTN1_{N169}$, and $MTN1_{N194}$ (Fig. S9*A*). Because the crystal structures of *Arabidopsis* MTN1 and MTN2 have been solved, we determined where the putative deamidation target residues are in relation to the MTN ligand-binding site and catalytic residues (Fig. 5*A*). $MTN1_{N113}$ is involved in ligand binding via coordination of a water molecule in the ligand-binding pocket (Fig. 5*A*) (71). $MTN1_{N194}$ and $MTN1_{N169}$ are both surface exposed at the end of helices α4 and α3, respectively (Fig. 5*A*). These conserved residues are located in approximately the same place in the MTN2 crystal structure (58).

To determine the effect of deamidation-mimicking mutations, we cloned and purified from *E. coli* the individual MTN1 variants $MTN1_{N113D}$, $MTN1_{N169D}$, and $MTN1_{N194D}$ and tested their activity in vitro (72). For negative controls, we also cloned and purified $MTN1_{D225N}$ and $MTN2_{D212N}$, which contain mutations in key catalytic residues (73). Both residues N113 and N194 resulted in loss-of-function phenotypes in MTN1 when converted to an aspartic acid (Fig. 5*B*). However, $MTN1_{N169D}$ retained wild-type levels of activity (Fig. 5*B*).

We then determined whether the loss-of-function phenotypes noted above were caused by mutations that mimic deamidation. We found that the $MTN1_{N194A}$ and $MTN1_{N194V}$ retained wild-type levels of activity in vitro (Fig. 5*B*). This finding suggests that the additional negative charge at $MTN1_{N194}$, as would occur during deamidation, causes a loss-of-function phenotype but that conservative replacement at $MTN1_{N194}$ does not alter activity. Conversely, $MTN1_{N113A}$ and $MTN1_{N113V}$ resulted in loss of function in vitro (Fig. 5*B*), suggesting that $MTN1_{N113}$ is sensitive to multiple mutations. Such sensitivity is consistent with the idea that $MTN1_{N113}$ is involved in ligand binding and therefore is a critical residue. We also generated the same set of variants for *Arabidopsis* MTN2 and determined that they function similarly to the MTN1 variants (Fig. 5*C*).

We generated *Arabidopsis* complementation lines using ubiquitin promoter (UBQ)-driven constructs of wild-type MTN1, $MTN1_{N194D}$, MTN_{N194V}, $MTN1_{N113D}$, $MTN1_{N113V}$, and $MTN1_{D225N}$ transformed into the *mtn1 mtn2* double mutant in the Col-0 background. The *mtn1 mtn2* double mutant is viable but fails to set seed (65). This sterility phenotype is unlikely to result from a defect in the Yang cycle, because *mtk* is not sterile. However, we did use this output as a tool to determine whether our complementation lines contain a functional copy of MTN1. It was previously demonstrated that UBQ promoter-driven MTN1 can complement the *mtn1 mtn2* reproductive and morphological defects (74). We generated T1 complementation lines and compared their developmental phenotypes with those of Col-0 and *mtn1 mtn2* plants (Fig. 5*D*). Wild-type MTN1 and $MTN1_{N194V}$ complemented the loss-of-seed-set phenotype, but the deamidation mimic $MTN1_{N194D}$ did not (Fig. 5*D*). Interestingly, the $MTN1_{N113V}$ complementation resulted in a range of phenotypes (Fig. S9*B*). Our control enzymatic loss-of-function complementation line $MTN1_{D225N}$ also remained sterile, similar to the *mtn1 mtn2* double mutant (Fig. 5*D*).

Discussion

Many plant bacterial pathogens use T3Es as virulence determinants. The type III secretion system is essential to the ability of these plant pathogens to cause disease in their hosts. However, many of the molecular mechanisms of type III effectors in virulence remain unknown. Understanding which host cellular systems T3Es target and how T3Es disrupt those systems will provide critical clues about the host cell physiology and defense machinery.

Here, we demonstrate a function for the *P. syringae* T3E HopAF1 and identify the Yang cycle as a previously unidentified component of the plant defense response. The presence of HopAF1 in multiple

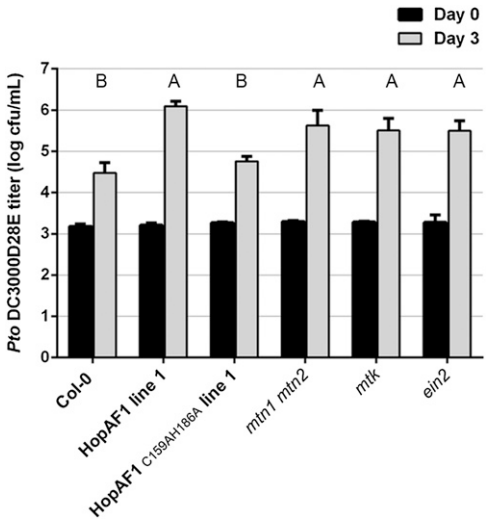

Fig. 4. *Arabidopsis* MTN1 and MTN2 play a role in ethylene-associated innate immunity pathways. Bacterial growth of *Pto* DC3000D28E in Col-0 plants and *mtn1 mtn2*, *mtk*, and *ein2* mutants was measured 0 and 3 d after hand-inoculation with bacteria (1×10^5 cfu/mL). Letters represent treatments with significant differences according to the post hoc ANOVA Tukey's test ($P < 0.05$).

strains of *P. syringae* and other plant pathogens suggests an important role in virulence. We propose a model (Fig. S10) wherein HopAF1 inhibits the host's Yang cycle proteins MTN1 and MTN2, leading to diminution of ethylene production and thereby contributing to suppression of PTI. We also demonstrate that MTN1, MTN2, and MTK are key components of the ethylene biosynthesis pathway when the plant immune system is activated.

HopAF1 is targeted to the plant plasma membrane, likely via acylation (Fig. 2). However, AvrXv3 does not contain the N-terminal acylation consensus sequences and consequently is found in the cytoplasm (Fig. 2 and Fig. S2*C*). This localization in the cytoplasm indicates that the plasma membrane localization of HopAF1 is not required for the function of this T3E family, because it is not evolutionarily maintained. This conclusion is consistent with our finding that HopAF1 interacts with the Yang cycle proteins MTN1 and MTN2. A specific localization of the Yang cycle has not been clearly delineated and, interestingly, we found MTN1 and MTN2 localized to both the plasma membrane and the cytoplasm (Fig. S6 *B* and *C*). This observation is consistent with published results showing that MTN1 can be found in both the cytoplasm and the plasma membrane, where it may interact with the calcineurin B-like protein CBL3 (60). We speculate that there are pools of *Arabidopsis* MTNs that cycle between the plasma membrane and cytoplasm and, therefore, there also are specific interactions between *Arabidopsis* MTNs and plasma membrane proteins. It is possible that HopAF1 has additional targets at the plasma membrane or that its ability to sequester MTNs to the plasma membrane inhibits a yet-to-be-discovered aspect of the Yang cycle.

A role for the Yang cycle in PTI responses is thus far undocumented. The Yang cycle kinase MTK was demonstrated to be required for the accumulation of high levels of ethylene by crossing *mtk* with an ethylene-overproducing mutant, *eto3* (59). This observation suggested that the Yang cycle is required for high levels of ethylene biosynthesis, such as occur during PTI. However, subsequent studies have suggested that the MTN proteins are not required for ethylene biosynthesis (65). Critically, these studies did not address ethylene accumulation in the double *mtn1 mtn2* mutant, nor did they attempt to induce high levels of ethylene accumulation (65). We postulated that the function of HopAF1 is to alter the function of MTN1 and MTN2, resulting in disruption of the Yang cycle and downstream PAMP-induced ethylene biosynthesis, and our data support this contention. We conclude that the Yang cycle is not required for steady-state levels of ethylene biosynthesis. However, our results show that MTN1 and MTN2 together, or MTK alone, are required for high levels of PAMP-induced ethylene biosynthesis

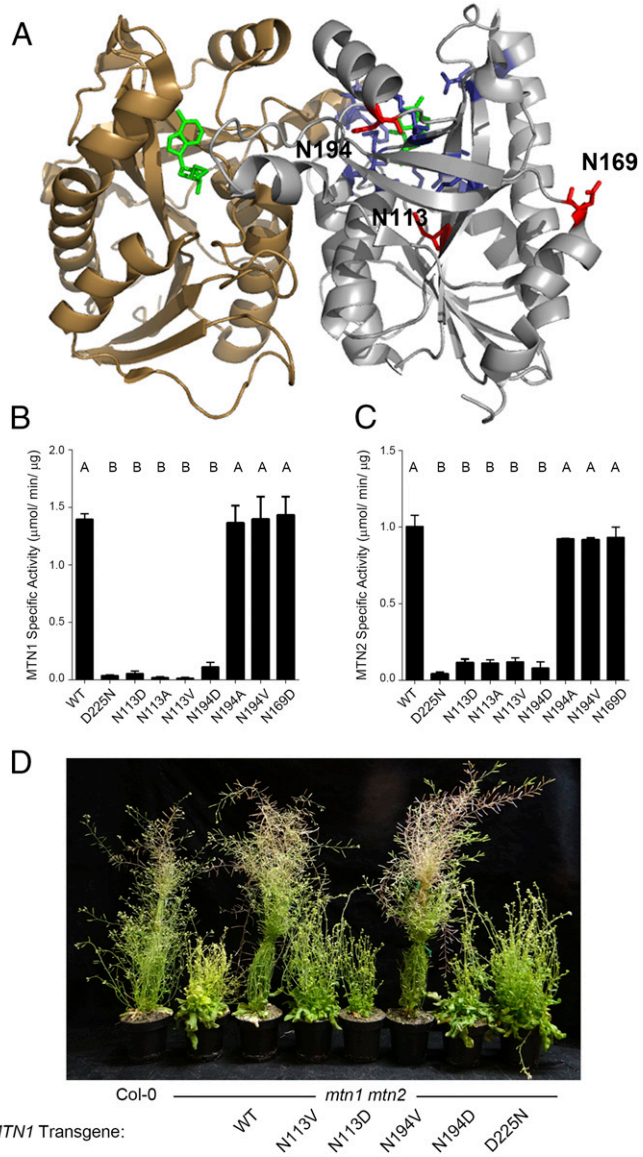

Fig. 5. Deamidation-mimicking variants of MTN1 and MTN2 lose the ability to cleave MTA in vitro. (*A*) Ribbon representation of the MTN1 crystal structure (PDB ID code 2H8G). Monomers are represented in sand and silver. The ligand analog (MTT) is shown in green. The ligand-binding and catalytic residues from MTN1 are represented as blue sticks. The putative conserved targets of deamidation are labeled and are shown as red sticks. Images were generated using PyMOL. (*B*) MTN1 enzyme-specific activity measured in vitro using a xanthine oxidase-coupled spectrometric assay. The MTN1 catalytic dead mutant is $MTN1_{D225N}$. (*C*) MTN2 enzyme-specific activity measured in vitro using a xanthine-oxidase coupled spectrometric assay. The MTN2 catalytic dead mutant is $MTN2_{D212N}$. Letters represent treatments with significant difference according to the post hoc ANOVA Tukey's test ($P < 0.05$). (*D*) *Arabidopsis* complementation lines in the *mtn1 mtn2* background that express UBQ:MTN variants at the T1 stage. UBQ:$MTN1_{N194D}$, UBQ:$MTN1_{N113D}$, and $MTN1_{D225N}$ complementation lines in the *mtn1 mtn2* background were not able complement the *mtn1 mtn2* sterile and stunted growth phenotype, suggesting that these MTN1 deamidation-mimic variants were nonfunctional.

and that HopAF1 inhibits ethylene biosynthesis by interacting with and targeting MTN1 and MTN2.

The role of ethylene in the plant defense response is well documented but is complicated because of the multiple, and sometimes conflicting, roles that ethylene might play in plant immune responses. For example, contradictory results from pathology assays might result from differences in the bacterial strains used and infection methods. Ethylene plays a role in defense against necrotrophs by antagonizing salicylic acid responses, which are involved in defense against biotrophs (75). Ethylene also is required for symptom development during infection with virulent and avirulent pathogens (76). Ethylene signaling also plays a role in PTI. Ethylene signaling directly controls *FLS2* expression by inducing the activation of the EIN3/EIL family of transcription factors, which directly bind the FLS2 promoter (68). This binding leads to an increase in FLS2 protein accumulation (68, 69). Mutants deficient in ethylene signaling pathways, such as *ein2*, have reduced *FLS2* transcript levels with or without flg22 treatment (68), likely contributing to the susceptibility of *ein2* mutants to weakened plant pathogens such as *Pto* DC3000 *ΔavrPto/ΔavrPtoB* (69). Furthermore, in tomatoes, XopD desumoylates and represses an ethylene-responsive transcription factor and suppresses ethylene accumulation (33). Ethylene also is required for the immune response against *X. campestris* pv. *euvesicatoria* (33). Thus, our findings with HopAF1 are consistent with emerging data suggesting that bacterial pathogens target various aspects of ethylene biology to manipulate their plant hosts (77).

HopAF1 is a member of the family of bacterial toxins/effectors that are able to deamidate specific substrates (Fig. 1). The C-terminal region of HopAF1 contains a fold that is homologous to bacterial deamidase proteins and contains the invariant catalytic residues C159 and H186A in the catalytic pocket. HopAF1 expression can block PTI (Fig. 1 *B* and *C*) and inhibit PAMP-induced ethylene biosynthesis that is dependent on an intact HopAF1 catalytic site (Fig. 3).

Although these data clearly demonstrate a genetic requirement of the predicted HopAF1 catalytic residues, we have been unable to demonstrate that HopAF1 deamidates *Arabidopsis* MTNs at the protein level or covalently modifies these host targets in any other way. We purified FLAG-tagged MTN1 coexpressed with HopAF1 from *N. benthamiana*. We obtained 100% peptide coverage of MTN1 following analysis of SDS/PAGE gel-excised tryptic fragments by LC-MS/MS but found no conclusive evidence for any modified peptides to support covalent modification by HopAF1. We noticed that transiently expressed MTN1-FLAG protein accumulated at lower levels when coexpressed with HopAF1 than with $HopAF1_{H186A}$, suggesting that MTN1 is potentially destabilized by HopAF1. However, this destabilization was not readily reversed by the addition of proteasome inhibitors coinoculated during the transient expression experiments. Additionally, we never observed cleavage products of MTN1 in the presence of HopAF1.

There are no known sequence/structural features to distinguish deamidases explicitly from other members of the papain-like superfamily (39), so we cannot preclude the possibility that HopAF1 is not a deamidase. However, CheD, a deamidase, accounts for five of the top 15 Meta server structural homology hits, and no other protein appears more than once. Additionally, although bacterial effectors/toxins that are deamidases have specific substrates, HopAF1 may deamidate a substrate in addition to *Arabidopsis* MTNs. Additional studies may reveal additional targets of HopAF1 deamidation.

In lieu of specific evidence that HopAF1 deamidates *Arabidopsis* MTNs, we generated *Arabidopsis* MTN deamidation-mimic variants at consensus conserved sites. Our results demonstrated that both $MTN1_{N113D}$ and $MTN1_{N194D}$, as well as the analogous mutations in MTN2, result in the loss of MTN activity in vitro and the inability to complement the *mtn1 mtn2* mutant phenotype *in planta*. Therefore, these residues are plausible targets of HopAF1 action (Fig. 5).

Multiple *P. syringae* T3Es target PTI signaling pathways using diverse biochemical mechanisms. In this study, we provide strong evidence for a molecular function of the common *P. syringae* T3E HopAF1. Additionally, we describe a new component of the plant innate immune system, the Yang cycle. We predict that effectors of the HopAF1 family target the Yang cycle proteins MTN1 and MTN2 (possibly by deamidation) to dampen ethylene production during bacterial infection. Future studies will be required to characterize the precise biochemical activity of HopAF1 in antagonizing MTN function.

Materials and Methods

Plant Lines and Growth Conditions. We used wild-type *A. thaliana* ecotype Columbia (Col-0). All mutants we used were in the Col-0 background. To generate the transgenic estradiol-inducible HopAF1-cerulean-HA and $HopAF1_{C159AH186A}$-cerulean-HA lines, the HopAF1 coding sequences were cloned into the pMDC7-cerulean-HA Gateway-compatible vector (78) and transformed into *Agrobacterium* GV3101. *Arabidopsis* transgenics were generated using *Agrobacterium*-mediated floral dip transformation (79). Hygromycin selection of transgenic plants was performed by growing seedlings on plates with 1/2 Murashige and Skoog medium with 15 μM hygromycin in the dark for 3 d and then in light conditions for 10 d. *mtn1-1* (65), *mtn1-2* (65), *mtn2-1* (65), *mtn2-2* (65), *mtn1-1 mtn2-1* (65), *mtk* (80), and *ein2-5* (67) strains were previously described. Except where otherwise noted, plants were grown under controlled short-day conditions (9 h light, 21 °C, 15 h dark, 18 °C). Tomato cultivars Fla 216 and Florida Fla 7060 have been described elsewhere (36).

Statistical Analysis. Histograms in all experiments, unless otherwise noted, were analyzed with ANOVA performed among all the samples, followed by Tukey's post hoc analysis ($P < 0.05$). Groups that differ significantly are indicated by different letters in the figures. Error bars represent SE.

Immunoblot Analysis of Plant Proteins. Unless otherwise noted, total proteins were extracted by grinding either fresh tissue or tissue flash-frozen in liquid nitrogen in a buffer containing 50 mM Tris·HCl (pH 8.0), 1% SDS, 1 mM EDTA, 14 mM β-mercaptoethanol, and 1 cOmplete protease inhibitor tablet (Roche) per 50 mL buffer. Samples were incubated on ice for 20 min; then the cell debris was pelleted by centrifuging the samples for 15 min at 20,800 × *g* at 4 °C. The supernatant was separated and quantified using the Bradford reagent. Protein was separated on 12% SDS/PAGE gels and transferred to a nitrocellulose membrane. Immunoblots were performed using standard methods. Anti-HA antibody (Santa Cruz Biotechnology) was used at a 1:5,000 dilution, anti-APX (Agrisera) was used at a 1:5,000 dilution, and anti–H^+-ATPase (Agrisera) was used at a 1:1,000 dilution. Anti-myc monoclonal antibody (Tissue Culture Facility, University of North Carolina) was used at a 1:5 dilution (81).

Homology Modeling. We initially detected the homology with the C-terminal domain of HopAF1 and CheD by querying the BioInfoBank Institute's Meta server and the HHPred structural prediction programs (41, 42). The 3D model for the HopAF1 C terminus structure based on the *T. maritima* CheD [Protein Data Bank (PDB) ID code 2F9Z] structure was generated with MODELER (82). The validity of the HopAF1 structural model was assessed using Verify3D (83). Graphical images and structural alignments were produced with PyMOL (84).

***Pto* DC3000D28E Growth Curve Assay.** Leaves of 5-wk-old plants were hand-inoculated with 1×10^5 cfu/mL of *Pto* DC3000D28E (47) resuspended in 10 mM $MgCl_2$. Leaf bacterial populations were determined on the day of inoculation and 3 d postinoculation. Each data point consisted of six replicates. Plants expressing either estradiol-inducible HopAF1-cerulean-HA or estradiol-inducible $HopAF1_{C159AH186A}$-cerulean-HA were sprayed with 20 μM estradiol 24 h before hand-inoculations.

Flg22-Dependent Pathogen Growth Inhibition Assay. Leaves of 5-wk-old plants were sprayed with 20 μM estradiol 12 h before flg22 infiltration. Plants were infiltrated with 1 μM flg22 or water 24 h before infiltration with 1×10^5 cfu/mL *Pto* DC3000. Leaf bacterial populations were determined at the indicated times. Each data point consisted of six replicates.

***Agrobacterium*-Mediated Transient Transformations in *N. benthamiana*.** Two microliters of overnight cultures were centrifuged at 10,000 × *g* for 1 min at room temperature. Cultures were resuspended in induction medium containing 10 mM $MgCl_2$ and 10 mM Mes (pH 5.5). Cultures were recentrifuged and then resuspended in induction medium plus 100 μM acetosyringone and were agitated at room temperature for 1 h. Cultures were diluted to the appropriate concentrations for each experiment and hand-infiltrated into fully expanded *N. benthamiana* leaves.

Coimmunoprecipitation. For coimmunoprecipitation experiments we generated 35S::MTN1-HA, 35S::MTN2-HA, 35S::HopAF1-myc, and 35S::HopAF1$_{H186A}$-myc using the Gateway constructs pGWB14 (C-terminal 3x-HA tag) and pGWB17 (C-terminal 4x-myc tag). Constructs were infiltrated at concentrations of 0.2 OD each with 0.1 OD P19 (85). Samples were collected and flash-frozen in liquid nitrogen. Protein was ground in lysis buffer [20 mM Tris·HCl (pH 8.0), 1 mM EDTA (pH 8.0), 150 mM NaCl, Roche cOmplete protease inhibitors] and centrifuged for 15 min at 6,000 × *g* in 4 °C. The supernatant was diluted to a concentration of 2 mg/mL. Anti-myc beads (50 μL) were added to the protein sample and incubated at 4 °C for 4 h with gentle agitation. The bound protein complexes were washed in extraction buffer [20 mM Tris·HCl (pH 8.0), 1 mM EDTA, 300 mM NaCl] and eluted in prewarmed 6x SDS/PAGE loading buffer. The input and bound proteins were analyzed by SDS/PAGE and immunoblot analysis.

Subcellular Localization. HopAF1, HopAF1$_{H186A}$, HopAF1$_{G2AC4S}$, AvrXv3, and AvrXv3$_{H126A}$ coding sequences were cloned into the Gateway-compatible pMDC7-cerulean-HA vector (78) and transferred into *Agrobacterium* strain C58C1 by triparental mating. *Agrobacterium*-mediated transformations in *N. benthamiana* leaves were performed as described above. *Agrobacterium* strains expressing HopAF1, HopAF1$_{H186A}$, HopAF1$_{G2AC4S}$, AvrXv3, or AvrXv3$_{H126A}$ were inoculated at an OD of 0.01 in combination with the PLC2 plasma membrane marker at 0.1 OD. Three days postinfiltration, leaves were sprayed with 5 μM estradiol. After 3 h, the subcellular localization of the proteins was observed using a Zeiss LSM 710 confocal scanning laser microscope. The plasma membrane marker PLC2-YFP was generated by cloning the PLC2 ORF from Col-0 cDNA into the pGWB41 Gateway vector.

Bimolecular Fluorescence Complementation. HopAF1 and MTN1 coding sequences were cloned into BiFC constructs that contain a UBQ promoter (86). HopAF1-nYFP, HopAF1$_{H186A}$-nYFP, or HopAF1$_{G2AC4S}$-nYFP was transiently coexpressed with MTN1-cYFP, MTN2-cYFP, or PLC2-cYFP in *N. benthamiana* leaves using *Agrobacterium*-mediated transient transformation. Strains expressing HopAF1, MTN1, MTN2, or PLC2 were inoculated at 0.4 OD with 0.1 OD of P19 (85). Confocal microscopy was used to image the reconstituted YFP signal 3 d after infiltration.

MTN Activity Assays. MTN activity assays were performed as previously described (72). Briefly, reactions were carried out in 50 mM imidazole (pH 8.0), 0.28 units of grade III buttermilk xanthine oxidase, 1 mM 2-(4-iodophenyl)-3-(4-nitrophenyl)-5-phenyltetrazolium chloride, and 0.12 μg recombinant MTN1. The reaction was monitored at 470 nm on a Tecan GENios microplate reader (Tecan, Ltd.) for 15 min with 1-min increments. Changes in absorbance were converted to the amount of adenine released using the molar absorption coefficient (15,400 M/cm at pH 8.0). To generate the Michaelis–Menten plot, the experiment was completed with a range of MTA concentrations [0–150 μM 5′-methylthioadenosine (MTA)]. Specific activity assays were completed with 50 μM MTA. All enzyme reactions had a final volume at 800 μL and were performed in triplicate at 25 °C. All reagents for the kinetic assay were purchased from Sigma-Aldrich Chemicals.

Ethylene Measurements. Leaves of adult (4- to 5-wk-old) plants were vacuum-infiltrated with *Pfo*-1 strains measured at OD 0.04 in 10 mM $MgCl_2$. After 3 h, the fresh weight of the seedlings was measured. Seedlings were sealed into gas chromatography vials, and ethylene was allowed to accumulate for 24 h. Ethylene accumulation was measured using a Clarus 500 gas chromatograph (PerkinElmer). A pure ethylene gas control was used in each experiment. Each data point represents three or four replicates.

ACKNOWLEDGMENTS. We thank members of the J.L.D. laboratory, especially Drs. David Hubert, Marc Nishimura, and Sarah Grant, for technical advice, helpful suggestions, and critical reading of the manuscript; Prof. Jeff Jones for plasmids and seeds; Prof. Margaret Sauter for antibodies and seeds; Tony Perdue for assistance with confocal microscopy; Gyeong Mee Yoon and Smadar Harpaz-saad for help with gas chromatography; and James Garzoni for greenhouse assistance. This work was funded by NIH Grant 1RO1 GM107444, Gordon and Betty Moore Foundation Grant GBMF3030, and National Science Foundation Grant IOS-1257373 (all to J.L.D.); NIH Training Grants T32 GM008581 (from the National Institute of General Medical Sciences) and T32 AI007273 (from the National Institute of Allergy and Infectious Diseases) (both to E.J.W.); NIH Dr. Ruth L. Kirschstein National Research Service Award Fellowship GM117758 (to O.M.F.); National Science Foundation Grant IOS 1456658 (to J.J.K.); and Biotechnology and Biological Sciences Research Council (UK) Grants BB/J004553/1 and BB/F008732/1 (both to M.J.B.). J.D.L. is an investigator of the Howard Hughes Medical Institute. M.J.B. is a fellow with the John Innes Foundation.

1. Grant SR, Fisher EJ, Chang JH, Mole BM, Dangl JL (2006) Subterfuge and manipulation: Type III effector proteins of phytopathogenic bacteria. *Annu Rev Microbiol* 60: 425–449.
2. Lindgren PB, Peet RC, Panopoulos NJ (1986) Gene cluster of Pseudomonas syringae pv. "phaseolicola" controls pathogenicity of bean plants and hypersensitivity of nonhost plants. *J Bacteriol* 168(2):512–522.
3. Ausubel FM (2005) Are innate immune signaling pathways in plants and animals conserved? *Nat Immunol* 6(10):973–979.
4. Boller T, Felix G (2009) A renaissance of elicitors: Perception of microbe-associated molecular patterns and danger signals by pattern-recognition receptors. *Annu Rev Plant Biol* 60:379–406.
5. Felix G, Duran JD, Volko S, Boller T (1999) Plants have a sensitive perception system for the most conserved domain of bacterial flagellin. *Plant J* 18(3):265–276.
6. Gómez-Gómez L, Boller T (2000) FLS2: An LRR receptor-like kinase involved in the perception of the bacterial elicitor flagellin in Arabidopsis. *Mol Cell* 5(6):1003–1011.
7. Felix G, Grosskopf DG, Regenass M, Basse CW, Boller T (1991) Elicitor-induced ethylene biosynthesis in tomato cells: Characterization and use as a bioassay for elicitor action. *Plant Physiol* 97(1):19–25.
8. Felix G, Grosskopf DG, Regenass M, Boller T (1991) Rapid changes of protein phosphorylation are involved in transduction of the elicitor signal in plant cells. *Proc Natl Acad Sci USA* 88(19):8831–8834.
9. Liu Y, Zhang S (2004) Phosphorylation of 1-aminocyclopropane-1-carboxylic acid synthase by MPK6, a stress-responsive mitogen-activated protein kinase, induces ethylene biosynthesis in Arabidopsis. *Plant Cell* 16(12):3386–3399.
10. Block A, et al. (2010) The Pseudomonas syringae type III effector HopG1 targets mitochondria, alters plant development and suppresses plant innate immunity. *Cell Microbiol* 12(3):318–330.
11. Jelenska J, van Hal JA, Greenberg JT (2010) Pseudomonas syringae hijacks plant stress chaperone machinery for virulence. *Proc Natl Acad Sci USA* 107(29):13177–13182.
12. Espinosa A, Guo M, Tam VC, Fu ZQ, Alfano JR (2003) The Pseudomonas syringae type III-secreted protein HopPtoD2 possesses protein tyrosine phosphatase activity and suppresses programmed cell death in plants. *Mol Microbiol* 49(2):377–387.
13. Feng F, et al. (2012) A Xanthomonas uridine 5′-monophosphate transferase inhibits plant immune kinases. *Nature* 485(7396):114–118.
14. Fu ZQ, et al. (2007) A type III effector ADP-ribosylates RNA-binding proteins and quells plant immunity. *Nature* 447(7142):284–288.
15. Kim HS, et al. (2005) The Pseudomonas syringae effector AvrRpt2 cleaves its C-terminally acylated target, RIN4, from Arabidopsis membranes to block RPM1 activation. *Proc Natl Acad Sci USA* 102(18):6496–6501.
16. López-Solanilla E, Bronstein PA, Schneider AR, Collmer A (2004) HopPtoN is a Pseudomonas syringae Hrp (type III secretion system) cysteine protease effector that suppresses pathogen-induced necrosis associated with both compatible and incompatible plant interactions. *Mol Microbiol* 54(2):353–365.
17. Shao F, et al. (2003) Cleavage of Arabidopsis PBS1 by a bacterial type III effector. *Science* 301(5637):1230–1233.
18. Gimenez-Ibanez S, et al. (2009) AvrPtoB targets the LysM receptor kinase CERK1 to promote bacterial virulence on plants. *Curr Biol* 19(5):423–429.
19. Göhre V, et al. (2008) Plant pattern-recognition receptor FLS2 is directed for degradation by the bacterial ubiquitin ligase AvrPtoB. *Curr Biol* 18(23):1824–1832.
20. Rosebrock TR, et al. (2007) A bacterial E3 ubiquitin ligase targets a host protein kinase to disrupt plant immunity. *Nature* 448(7151):370–374.
21. Shan L, et al. (2008) Bacterial effectors target the common signaling partner BAK1 to disrupt multiple MAMP receptor-signaling complexes and impede plant immunity. *Cell Host Microbe* 4(1):17–27.
22. Xiang T, et al. (2008) Pseudomonas syringae effector AvrPto blocks innate immunity by targeting receptor kinases. *Curr Biol* 18(1):74–80.
23. Zhou J, et al. (2014) The Pseudomonas syringae effector HopF2 suppresses Arabidopsis immunity by targeting BAK1. *Plant J* 77(2):235–245.
24. Wang Y, et al. (2010) A Pseudomonas syringae ADP-ribosyltransferase inhibits Arabidopsis mitogen-activated protein kinase kinases. *Plant Cell* 22(6):2033–2044.
25. Zhang J, et al. (2007) A Pseudomonas syringae effector inactivates MAPKs to suppress PAMP-induced immunity in plants. *Cell Host Microbe* 1(3):175–185.
26. Nicaise V, et al. (2013) Pseudomonas HopU1 modulates plant immune receptor levels by blocking the interaction of their mRNAs with GRP7. *EMBO J* 32(5):701–712.
27. Zhou H, et al. (2011) Pseudomonas syringae type III effector HopZ1 targets a host enzyme to suppress isoflavone biosynthesis and promote infection in soybean. *Cell Host Microbe* 9(3):177–186.
28. Nomura K, et al. (2006) A bacterial virulence protein suppresses host innate immunity to cause plant disease. *Science* 313(5784):220–223.

29. Dodds PN, Rathjen JP (2010) Plant immunity: Towards an integrated view of plant-pathogen interactions. *Nat Rev Genet* 11(8):539–548.
30. Jones JD, Dangl JL (2006) The plant immune system. *Nature* 444(7117):323–329.
31. Pieterse CM, Leon-Reyes A, Van der Ent S, Van Wees SC (2009) Networking by small-molecule hormones in plant immunity. *Nat Chem Biol* 5(5):308–316.
32. Cohn JR, Martin GB (2005) Pseudomonas syringae pv. tomato type III effectors AvrPto and AvrPtoB promote ethylene-dependent cell death in tomato. *Plant J* 44(1): 139–154.
33. Kim JG, Stork W, Mudgett MB (2013) Xanthomonas type III effector XopD desumoylates tomato transcription factor SlERF4 to suppress ethylene responses and promote pathogen growth. *Cell Host Microbe* 13(2):143–154.
34. Chang JH, et al. (2005) A high-throughput, near-saturating screen for type III effector genes from Pseudomonas syringae. *Proc Natl Acad Sci USA* 102(7):2549–2554.
35. Baltrus DA, et al. (2011) Dynamic evolution of pathogenicity revealed by sequencing and comparative genomics of 19 Pseudomonas syringae isolates. *PLoS Pathog* 7(7): e1002132.
36. Astua-Monge G, et al. (2000) Resistance of tomato and pepper to T3 strains of Xanthomonas campestris pv. vesicatoria is specified by a plant-inducible avirulence gene. *Mol Plant Microbe Interact* 13(9):911–921.
37. Potnis N, et al. (2011) Comparative genomics reveals diversity among xanthomonads infecting tomato and pepper. *BMC Genomics* 12:146.
38. Studholme DJ, et al. (2010) Genome-wide sequencing data reveals virulence factors implicated in banana Xanthomonas wilt. *FEMS Microbiol Lett* 310(2):182–192.
39. Washington EJ, Banfield MJ, Dangl JL (2013) What a difference a Dalton makes: Bacterial virulence factors modulate eukaryotic host cell signaling systems via deamidation. *Microbiol Mol Biol Rev* 77(3):527–539.
40. Markowitz VM, et al. (2012) IMG: The Integrated Microbial Genomes database and comparative analysis system. *Nucleic Acids Res* 40(Database issue):D115–D122.
41. Bujnicki JM, Elofsson A, Fischer D, Rychlewski L (2001) Structure prediction meta server. *Bioinformatics* 17(8):750–751.
42. Söding J, Biegert A, Lupas AN (2005) The HHpred interactive server for protein homology detection and structure prediction. *Nucleic Acids Res* 33(Web Server issue): W244-8.
43. Chao X, et al. (2006) A receptor-modifying deamidase in complex with a signaling phosphatase reveals reciprocal regulation. *Cell* 124(3):561–571.
44. Flatau G, et al. (1997) Toxin-induced activation of the G protein p21 Rho by deamidation of glutamine. *Nature* 387(6634):729–733.
45. Schmidt G, et al. (1997) Gln 63 of Rho is deamidated by Escherichia coli cytotoxic necrotizing factor-1. *Nature* 387(6634):725–729.
46. Jamir Y, et al. (2004) Identification of Pseudomonas syringae type III effectors that can suppress programmed cell death in plants and yeast. *Plant J* 37(4):554–565.
47. Cunnac S, et al. (2011) Genetic disassembly and combinatorial reassembly identify a minimal functional repertoire of type III effectors in Pseudomonas syringae. *Proc Natl Acad Sci USA* 108(7):2975–2980.
48. Zipfel C, et al. (2004) Bacterial disease resistance in Arabidopsis through flagellin perception. *Nature* 428(6984):764–767.
49. Resh MD (2006) Trafficking and signaling by fatty-acylated and prenylated proteins. *Nat Chem Biol* 2(11):584–590.
50. Nimchuk Z, et al. (2000) Eukaryotic fatty acylation drives plasma membrane targeting and enhances function of several type III effector proteins from Pseudomonas syringae. *Cell* 101(4):353–363.
51. Shan L, Thara VK, Martin GB, Zhou JM, Tang X (2000) The pseudomonas AvrPto protein is differentially recognized by tomato and tobacco and is localized to the plant plasma membrane. *Plant Cell* 12(12):2323–2338.
52. Robert-Seilaniantz A, Shan L, Zhou JM, Tang X (2006) The Pseudomonas syringae pv. tomato DC3000 type III effector HopF2 has a putative myristoylation site required for its avirulence and virulence functions. *Mol Plant Microbe Interact* 19(2):130–138.
53. Lewis JD, Abada W, Ma W, Guttman DS, Desveaux D (2008) The HopZ family of Pseudomonas syringae type III effectors require myristoylation for virulence and avirulence functions in Arabidopsis thaliana. *J Bacteriol* 190(8):2880–2891.
54. Dowen RH, Engel JL, Shao F, Ecker JR, Dixon JE (2009) A family of bacterial cysteine protease type III effectors utilizes acylation-dependent and -independent strategies to localize to plasma membranes. *J Biol Chem* 284(23):15867–15879.
55. Otterhag L, Sommarin M, Pical C (2001) N-terminal EF-hand-like domain is required for phosphoinositide-specific phospholipase C activity in Arabidopsis thaliana. *FEBS Lett* 497(2-3):165–170.
56. Mukhtar MS, et al.; European Union Effectoromics Consortium (2011) Independently evolved virulence effectors converge onto hubs in a plant immune system network. *Science* 333(6042):596–601.
57. Miyazaki JH, Yang SF (1987) Metabolism of 5-methylthioribose to methionine. *Plant Physiol* 84(2):277–281.
58. Park EY, et al. (2009) Biochemical and structural characterization of 5′-methylthioadenosine nucleosidases from Arabidopsis thaliana. *Biochem Biophys Res Commun* 381(4): 619–624.
59. Bürstenbinder K, Rzewuski G, Wirtz M, Hell R, Sauter M (2007) The role of methionine recycling for ethylene synthesis in Arabidopsis. *Plant J* 49(2):238–249.
60. Oh SI, et al. (2008) The Arabidopsis calcium sensor calcineurin B-like 3 inhibits the 5′-methylthioadenosine nucleosidase in a calcium-dependent manner. *Plant Physiol* 148(4):1883–1896.
61. Grefen C, et al. (2010) A ubiquitin-10 promoter-based vector set for fluorescent protein tagging facilitates temporal stability and native protein distribution in transient and stable expression studies. *Plant J* 64(2):355–365.
62. Marmagne A, et al. (2007) A high content in lipid-modified peripheral proteins and integral receptor kinases features in the arabidopsis plasma membrane proteome. *Mol Cell Proteomics* 6(11):1980–1996.
63. Thomas WJ, Thireault CA, Kimbrel JA, Chang JH (2009) Recombineering and stable integration of the Pseudomonas syringae pv. syringae 61 hrp/hrc cluster into the genome of the soil bacterium Pseudomonas fluorescens Pf0-1. *Plant J* 60(5):919–928.
64. Mudgett MB, Staskawicz BJ (1999) Characterization of the Pseudomonas syringae pv. tomato AvrRpt2 protein: Demonstration of secretion and processing during bacterial pathogenesis. *Mol Microbiol* 32(5):927–941.
65. Bürstenbinder K, et al. (2010) Inhibition of 5′-methylthioadenosine metabolism in the Yang cycle alters polyamine levels, and impairs seedling growth and reproduction in Arabidopsis. *Plant J* 62(6):977–988.
66. Kushad MM, Richardson DG, Ferro AJ (1985) 5′-Methylthioadenosine Nucleosidase and 5-Methylthioribose Kinase Activities and Ethylene Production during Tomato Fruit Development and Ripening. *Plant Physiol* 79(2):525–529.
67. Alonso JM, Hirayama T, Roman G, Nourizadeh S, Ecker JR (1999) EIN2, a bifunctional transducer of ethylene and stress responses in Arabidopsis. *Science* 284(5423): 2148–2152.
68. Boutrot F, et al. (2010) Direct transcriptional control of the Arabidopsis immune receptor FLS2 by the ethylene-dependent transcription factors EIN3 and EIL1. *Proc Natl Acad Sci USA* 107(32):14502–14507.
69. Mersmann S, Bourdais G, Rietz S, Robatzek S (2010) Ethylene signaling regulates accumulation of the FLS2 receptor and is required for the oxidative burst contributing to plant immunity. *Plant Physiol* 154(1):391–400.
70. Cornell KA, Swarts WE, Barry RD, Riscoe MK (1996) Characterization of recombinant Eschericha coli 5′-methylthioadenosine/S-adenosylhomocysteine nucleosidase: Analysis of enzymatic activity and substrate specificity. *Biochem Biophys Res Commun* 228(3):724–732.
71. Siu KK, et al. (2008) Molecular determinants of substrate specificity in plant 5′-methylthioadenosine nucleosidases. *J Mol Biol* 378(1):112–128.
72. Dunn SM, Bryant JA, Kerr MW (1994) A simple spectrophotometric assay for plant 5′-deoxy-5′-methylthioadenosine nucleosidase using xanthine oxidase as a coupling enzyme. *Phytochem Anal* 5:286–290.
73. Bretes E, Guranowski A, Nuc K (2011) 5′-methylthioadenosine nucleosidase from yellow lupine (Lupinus luteus): Molecular characterization and mutational analysis. *Protein Pept Lett* 18(8):817–824.
74. Waduwara-Jayabahu I, et al. (2012) Recycling of methylthioadenosine is essential for normal vascular development and reproduction in Arabidopsis. *Plant Physiol* 158(4): 1728–1744.
75. Robert-Seilaniantz A, Navarro L, Bari R, Jones JD (2007) Pathological hormone imbalances. *Curr Opin Plant Biol* 10(4):372–379.
76. Bent AF, Innes RW, Ecker JR, Staskawicz BJ (1992) Disease development in ethylene-insensitive Arabidopsis thaliana infected with virulent and avirulent Pseudomonas and Xanthomonas pathogens. *Mol Plant Microbe Interact* 5(5):372–378.
77. Broekaert WF, Delauré SL, De Bolle MF, Cammue BP (2006) The role of ethylene in host-pathogen interactions. *Annu Rev Phytopathol* 44:393–416.
78. Akimoto-Tomiyama C, et al. (2012) XopR, a type III effector secreted by Xanthomonas oryzae pv. oryzae, suppresses microbe-associated molecular pattern-triggered immunity in Arabidopsis thaliana. *Mol Plant Microbe Interact* 25(4):505–514.
79. Clough SJ, Bent AF (1998) Floral dip: A simplified method for Agrobacterium-mediated transformation of Arabidopsis thaliana. *Plant J* 16(6):735–743.
80. Sauter M, Cornell KA, Beszteri S, Rzewuski G (2004) Functional analysis of methylthioribose kinase genes in plants. *Plant Physiol* 136(4):4061–4071.
81. Boyes DC, Nam J, Dangl JL (1998) The Arabidopsis thaliana RPM1 disease resistance gene product is a peripheral plasma membrane protein that is degraded coincident with the hypersensitive response. *Proc Natl Acad Sci USA* 95(26):15849–15854.
82. Sali A, Blundell TL (1993) Comparative protein modelling by satisfaction of spatial restraints. *J Mol Biol* 234(3):779–815.
83. Eisenberg D, Lüthy R, Bowie JU (1997) VERIFY3D: Assessment of protein models with three-dimensional profiles. *Methods Enzymol* 277:396–404.
84. The PyMol Molecular Graphics System, Version 1.5.0.5 (Schrodinger, LLC, New York).
85. Voinnet O, Rivas S, Mestre P, Baulcombe D (2003) An enhanced transient expression system in plants based on suppression of gene silencing by the p19 protein of tomato bushy stunt virus. *Plant J* 33(5):949–956.
86. Gehl C, Waadt R, Kudla J, Mendel RR, Hänsch R (2009) New GATEWAY vectors for high throughput analyses of protein-protein interactions by bimolecular fluorescence complementation. *Mol Plant* 2(5):1051–1058.
87. Altschul SF, Gish W, Miller W, Myers EW, Lipman DJ (1990) Basic local alignment search tool. *J Mol Biol* 215(3):403–410.
88. Edgar RC (2004) MUSCLE: Multiple sequence alignment with high accuracy and high throughput. *Nucleic Acids Res* 32(5):1792–1797.
89. Jones DT, Taylor WR, Thornton JM (1992) The rapid generation of mutation data matrices from protein sequences. *Comput Appl Biosci* 8(3):275–282.
90. Felsenstein J (1985) Confidence limits on phylogenies: An approach using the bootstrap. *Evolution* 39(4):783–791.
91. Tamura K, Stecher G, Peterson D, Filipski A, Kumar S (2013) MEGA6: Molecular Evolutionary Genetics Analysis version 6.0. *Mol Biol Evol* 30(12):2725–2729.
92. Letunic I, Bork P (2007) Interactive Tree Of Life (iTOL): An online tool for phylogenetic tree display and annotation. *Bioinformatics* 23(1):127–128.
93. Aslanidis C, de Jong PJ (1990) Ligation-independent cloning of PCR products (LIC-PCR). *Nucleic Acids Res* 18(20):6069–6074.
94. Rzewuski G, et al. (2007) OsMTN encodes a 5′-methylthioadenosine nucleosidase that is up-regulated during submergence-induced ethylene synthesis in rice (Oryza sativa L.). *J Exp Bot* 58(6):1505–1514.
95. Siu KK, et al. (2011) Mechanism of substrate specificity in 5′-methylthioadenosine/S-adenosylhomocysteine nucleosidases. *J Struct Biol* 173(1):86–98.